npj Climate and Atmospheric Science https://doi.org/10.1038/s41612-026-01440-6

Article in Press

Interannual variations in terrestrial carbon uptake are dominated by temperature and the vapor pressure deficit rather than water availability

Received: 26 January 2026

Accepted: 13 May 2026

Cite this article as: Jiang, D., Yu, Z., Wang, J. *et al.* Interannual variations in terrestrial carbon uptake are dominated by temperature and the vapor pressure deficit rather than water availability. *npj Clim Atmos Sci* (2026). https://doi.org/10.1038/s41612-026-01440-6

Dong Jiang, Zhe Yu, Jianhua Wang, Mengmeng Hao, Xingxing Zhang, Xiaoxi Yan, Jinglei Liu, Zhaoxing Li & Zhaofei Liu

Interannual variations in terrestrial carbon uptake are dominated by temperature and the vapour pressure deficit rather than water availability

Submitted to: npj Climate and Atmospheric Science

By

Dong Jiang[1, 3*], Zhe Yu[1, 3], Jianhua Wang[2*], Mengmeng Hao[1, 3], Xingxing Zhang[1, 3], Xiaoxi Yan[4], Jinglei Liu[1, 3], Zhaoxing Li[1, 3], Zhaofei Liu[1, 3*]

[1] Institute of Geographic Sciences and Natural Resources Research, Chinese Academy of Sciences, 100101, Beijing, China

[2] State Key Laboratory of Simulation and Regulation of Water Cycle in River Basin, China Institute of Water Resources and Hydropower Research, 100038, Beijing, China

[3] University of Chinese Academy of Sciences, 100049, Beijing, China

[4] State Key Laboratory of Remote Sensing and Digital Earth, Aerospace Information Research Institute, Chinese Academy of Sciences, 100101, Beijing, China

*Corresponding author, Dong Jiang (jiangd@igsnrr.ac.cn); Jianhua Wang (wjh@iwhr.com); and Zhaofei Liu (zfliu@igsnrr.ac.cn)

May 7, 2026

Abstract

Interannual variations in terrestrial carbon uptake (IVTCU) strongly regulate anthropogenic CO_2 growth rate dynamics, yet their controlling mechanisms remain uncertain. Previous studies disagree on whether precipitation (P) or temperature (T) predominates and whether soil moisture (SM) or vapour pressure deficit (VPD) is the primary driver. Using ground-based meteorological observations and remotely sensed gross carbon uptake data (1982-2016), we reveal that the global IVTCU are controlled by T and VPD, whereas the influences of water availability (P or SM) are relatively weak. Regionally, the VPD exerts dominant control in arid areas and common drought-adapted ecosystems, whereas T predominates in other regions, especially cold areas. In contrast to the prevailing view that water availability constrains carbon uptake in arid systems, our analysis reveals that although P yields greater influences in these regions than elsewhere, the VPD remains the main factor limiting the IVTCU. This highlights the notable inhibitory effect of atmospheric dryness on arid ecosystem carbon uptake. Globally, the sensitivity of the IVTCU to T is greatest between 7°C and 16°C and decreases rapidly at higher T, where the VPD gradually becomes the dominant factor. The IVTCU respond less strongly to the VPD than to T, but the VPD maintains a substantial influence, especially below 10 hPa. Both the sensitivity and threshold vary across land cover/climate zones. These findings refine our understanding of the mechanisms driving carbon flux variability, challenge conventional assumptions regarding arid-region controls, and provide critical insights for improving land–atmosphere coupling models under a changing climate.

INTRODUCTION

Terrestrial ecosystems are a core component of the global carbon cycle and play an indispensable role in mitigating global warming. By absorbing approximately 25% of anthropogenic CO_2 emissions, they also help maintain the global carbon budget[1,2]. The interannual variations in terrestrial carbon uptake (IVTCU) serve as key regulatory links between terrestrial ecosystems and atmospheric CO_2 mitigation, as indicated by the dynamic fluctuations in the net carbon sequestration capacity of terrestrial ecosystems across years[3].

The IVTCU are driven primarily by plant photosynthesis, which can be directly affected by temperature (T) and soil moisture (SM) or indirectly affected by the vapour pressure deficit (VPD) through the control of stomatal opening. While many studies have focused on investigating the influence of the aforementioned factors on the IVTCU, the conclusions remain highly inconsistent. Debates first manifested in the fundamental question of whether the IVTCU are controlled mainly by T or water availability (e.g., precipitation or SM). Some studies have argued that, on the basis of terrestrial carbon data from remote sensing or model simulations, precipitation (P) functions as a more dominant driver of carbon fluxes than T[4-7]. In addition, large influences of SM on the interannual variability in terrestrial carbon uptake have been identified by climate or earth system model simulations[1,3]. Some studies have emphasized that T exerts a stronger influence on the global carbon fluxes than P does, but the strength of this T-driven response can conversely be modulated by P[8,9]. Other studies have reported that T and P have comparable effects on the global IVTCU[10]. Regional analyses further revealed that the dominant drivers of terrestrial carbon fluxes vary by ecosystem type: the dominant drivers can be P or SM in arid land ecosystems[11,12] or T in

tropical ecosystems[10,13].

More recent studies have reported that the VPD might be the main driving factor of the IVTCU. On the basis of surface flux observations, reanalysis meteorological data and remote sensing vegetation data, an increase in the VPD with decreasing stomatal conductance was concluded to be the main cause of the reduction in global and regional terrestrial carbon uptake[14-17]. On the basis of similar data sources, increases in the VPD rather than changes in P substantially influence grassland productivity[18]. Compared with other environmental variables (e.g., T, P, and SM), the VPD has been observed to have persistent and widespread effects on terrestrial carbon uptake through a partial correlation analysis[2]. The stronger VPD constraint compared with the T enhancement of the global gross primary productivity (GPP) has been identified by stepwise regression analysis[19]. Conversely, reanalysis and remote sensing data have revealed that warming-induced increases in the VPD do not suppress vegetation growth in northern peatlands[20]. In addition, a divergent response of productivity to the VPD has also been discovered in the Northern Hemisphere when the interactive effects of the VPD with T and SM are excluded[21].

The inconsistencies in the dominant drivers of carbon fluxes may stem from the adoption of different datasets. For example, terrestrial water storage (TWS) and T have been identified as the dominant drivers on the basis of the GPP data of TRENDY and FluxCom, respectively[22]. This might be because of the opposite trends in the two GPP datasets (Supplementary Fig. 1). However, similar datasets and methods may also yield opposing results. For example, SM was identified as the dominant driver of dryness stress on ecosystem production across more than 70% of vegetated land areas using solar-induced fluorescence and reanalysis datasets[12]. In contrast, compared with

similar SM-based data and methods, the VPD has been found to exert greater and wider effects on ecosystem production efficiency[23].

Data are crucial for research results. Previous studies on the influencing factors of carbon fluxes in terrestrial ecosystems have relied mainly on simulated and reanalysis meteorological data products, which often diverge substantially from ground observations in terms of not only the values themselves (Supplementary Fig. 2) but also the trends (Supplementary Fig. 3). The different data used in these studies might explain the significant disparity in the dominant factor attributions of the IVTCU.

To provide a more comprehensive understanding of the influencing mechanism of the IVTCU, we systematically evaluated the impacts of T, VPD, and P on the terrestrial gross carbon uptake (1982-2016), as well as the variations within climate and land cover zones, on the basis of the ground-observed meteorological data closest to the true values and satellite-based GPP datasets with different trends. Our results can deepen the understanding of the mechanisms influencing global and regional terrestrial carbon uptake changes and enhance the rationality of coupled land–atmosphere simulations against the background of climate change.

RESULTS

Global IVTCU are dominated by T and the VPD rather than P or SM

Significant differences in the VPD were identified between ground observations and various reanalysis datasets (Supplementary Table 1, Supplementary Figs. 2 and 3). Therefore, ground observations were utilized to provide a more reliable assessment of the effects of meteorological factors, such as the VPD, on the terrestrial gross carbon uptake. For the GPP datasets, although

most (11/18) GPP products (Supplementary Table 2) show increasing trends, seven GPP products show decreasing trends (Supplementary Fig. 3). Nine remotely sensed GPP products with relatively long periods (1982–2016) were adopted to generate ensemble mean GPP data series for the grids where each ground meteorological observation station is located.

On the basis of ground observations and the ensemble mean GPP data, we applied a ridge regression model to evaluate the impact of meteorological factors on the IVTCU for each observation station (Fig. 1). The overall ridge regression coefficients (RRCs) of the VPD, P, and T with respect to GPP were -0.52 ± 0.37 (mean ± 1 standard error), 0.11 ± 0.15, and 0.60 ± 0.40, respectively. Despite the strong inhibitory effect of the VPD on the IVTCU, T had a stronger effect on the IVTCU and was identified as the dominant factor for the IVTCU at 53.2% of the stations (525/986), whereas the VPD was found to be the dominant factor at 42.5% of the stations (419/986). This finding differs from the previous understanding that the VPD or SM were the dominant factors affecting the IVTCU in the past decade.

The impacts of the VPD and T on the IVTCU exhibited strong latitudinal distributions (Fig. 1). From north to south, the influence of T on IVTCU gradually decreases, whereas the influence of the VPD generally tends to increase. In the boreal and subboreal regions (latitude ≥ 50°N), 79.7% (220/276) of the stations revealed T as the dominant factor, indicating that T was the dominant factor influencing the IVTCU. The VPD was found to be the dominant factor at 54 stations in these regions, and the majority (46/54) were distributed between 50 and 55°N. This is mainly because the scarcity of heat resources makes T more important for vegetation growth in these regions. In the temperate regions (24–49°N), the main controlling factors influencing the IVTCU were the

VPD and T, with 48.2% (308/639) and 47.1% (301/639) of the stations showing the VPD and T as the dominant factor, respectively. The dominant factor of the VPD was located mainly in the arid and semiarid grasslands of Eurasia and North America. The dominant role of the VPD in shaping the IVTCU was also found mainly in the tropics and the Southern Hemisphere, with the corresponding station proportion increasing to 80.3% (57/71). The proportions of stations where P and T were the dominant factors in these regions were 14.1% (10/71) and 5.6% (4/71), respectively. This is due mainly to the diversity of interannual trends in GPP and its influencing factors (Supplementary Fig. 4). For example, although T at most global stations has shown significant increasing trends, the trends in the Southern Hemisphere differ. Evaluations based on individual GPP products also yielded similar results (Supplementary Fig. 5).

In this study, the impacts of SM, the VPD, and T on the IVTCU (Supplementary Figs. 6 and 7) were also assessed on the basis of the ensemble mean series of three satellite and reanalysis SM data products (Supplementary Table 3). The impact of SM on the IVTCU was generally lower than that of T and the VPD. The RRCs between SM and GPP were concentrated mainly between 0.15 and 0.40, with a mean of 0.28 (Supplementary Fig. 6). Overall, the spatial distribution of the RRCs between SM and GPP (Supplementary Fig. 7) was essentially consistent with that between P and GPP (Fig. 1-c and g). This indicated that the influences of P and SM, which represent water availability, on the IVTCU are similar.

Fig. 1

Dominant factors of the IVTCU: the VPD in zones with drought-adapted ecosystems and T in other zones, especially for boreal areas and forests

Inspired by the spatial variations in the dominant factors of the IVTCU (Fig. 1), we further calculated the variations in the dominant factors across different land cover types and climate zones (Fig. 2). Zones, including the tropical rainforest and tropical monsoon climate zones, as well as the wetlands and barren land cover zones, were not analysed because of insufficient observation stations (<20 stations). The inhibitory effect of the VPD on the IVTCU was highest in the arid steppe zone, with median RRCs of approximately -0.80. The positive effect of T on the IVTCU was strongest in the three cold zones (e.g., CDS, CDW, and CWDS), with median RRCs > 0.80. Despite the generally weaker effects than that exhibited by T, P had a larger influence in the arid desert zone, with a higher median RRC, indicating that, in arid areas, the influence of water availability on vegetation is greater than that of T.

Fig. 2

The VPD was found to play a dominant role in shaping the IVTCU in arid climate zones, including arid desert, arid steppe, temperate dry summer, temperate dry winter, and tropical savannah, with the share of VPD-dominant stations being 68.4% (13/19), 71.4% (90/126), 66.7% (20/30), 53.7% (22/41), and 88.6% (31/35), respectively. These climate zones are mainly characterized by drought-adapted ecosystems. T was observed as the dominant factor affecting the IVTCU in the other five climate zones (e.g., TWDS, CDS, CDW, CWDS, and Polar), with all the

proportions of T-dominant stations above 70%, indicating that under these climate conditions, the effect of the VPD on the IVTCU through stomatal closure weakened, while the impact of T became more dominant.

With respect to land cover types, the inhibitory effect of the VPD on the IVTCU was strongest in grassland, cropland and shrubland ecosystems, with median RRCs < -0.50, and lowest in forestland and savanna ecosystems, with both median RRCs > -0.35. The positive effect of T on the IVTCU was strongest in the forest ecosystem, with the median RRC reaching 0.84, and weakest in the shrubland ecosystem, with the median RRC being only 0.32. The positive effect of P on the IVTCU of all land cover types was generally weak, with all the median RRCs < 0.15. Similar to the assessment results of climate zones, the dominant role of the VPD in determining the IVTCU was also identified in grassland, cropland and shrubland ecosystems, with drought as a common feature, for 59.2% (151/255), 49.7% (168/338) and 61.1% (11/18) of the stations, respectively. This might be due to the stronger sensitivity of grassland ecosystems to the VPD. The dominant role of T in shaping the IVTCU was identified in the other three land cover types, including forests, savannas, and urban and built-up areas, with the proportions of stations being 89.9% (80/89), 69.6% (165/237), and 51.1% (23/45), respectively.

The assessment results of SM, the VPD, and T were essentially consistent with those of P, the VPD, and T. T was identified as the dominant factor on the IVTCU in the cold and temperate humid regions, whereas the VPD was the dominant factor in the four arid regions of the warm and temperate zones (e.g., tropical savannah, arid desert, arid steppe, and temperate dry summer), with a share of 55.5% (101/182 stations). SM also had a stronger influence on the IVTCU in these four

arid regions than in the other regions, with a proportion of 28.0% (51/182) of the stations where SM was dominant.

Sensitivity of the IVTCU to T and the VPD and their critical thresholds

Overall, the impact of T on the IVTCU gradually decreased as T increased but showed two critical threshold inflection points at 7°C and 16°C (Fig. 3). Both of critical thresholds were statistical significant at a significance level of 0.05 (same as following). When T was less than 7°C, the rate of change of the RRC decreased, indicating a relatively lower sensitivity of the IVTCU to T. However, with a relatively high RRC of approximately 0.6, T could be further confirmed as the dominant factor for the IVTCU under low-temperature conditions. When T varied between 7°C and 16°C, the mean RRC to IVTCU decreased from 0.54 to 0.18, demonstrating a significant reduction in the impact of T on vegetation growth changes as temperature increased. When T was greater than 16°C, the effect of T on the IVTCU continued to decrease but with a much lower rate of change than at 7–16°C. When T reached 13°C, 15°C, and 20°C, the mean RRCs of T decreased to less than 0.30, 0.20, and 0.10, respectively, which were lower than the mean RRC of the VPD, indicating that the impact of T on the IVTCU generally became lower than that of the VPD under these temperature conditions. In other words, the effect of the VPD on the IVTCU became increasingly dominant when T > 13°C, whereas T lost its dominant role. Overall, the sensitivity of the IVTCU to T within the range of 7°C to 16°C was significantly greater than that in other T ranges. When T became greater than the average T of all the stations (approximately 10°C), the

factor dominating the IVTCU began to shift from T to the VPD as the mean RRC of T decreased below that of the VPD (approximately 0.40).

Fig. 3

The VPD displayed an overall strong inhibitory effect on the IVTCU, with the mean RRC being less than -0.33 for each calculation bin (Fig. 3-b). The threshold statistical significant inflection points in the sensitivity of the IVTCU to VPD occurred at 2.5 hPa, 7.0 hPa, and 10.0 hPa. Below 10.0 hPa, the VPD strongly inhibited the IVTCU, with the mean RRCs ranging from -0.55 to -0.50, and exhibited a trend of strengthening–weakening–strengthening. At this stage, the sensitivity of the IVTCU to the VPD was relatively low. Above 10.0 hPa, the sensitivity of the IVTCU to high VPD values (> 10.0 hPa) was relatively high. The inhibitory effect of the VPD decreased more rapidly with increasing VPD, especially when the VPD was above 15 hPa.

The sensitivity and thresholds under different land cover types and climate zones were also analysed (Fig. 4). The impact of T on the IVTCU for all land cover types generally decreased as T increased (Fig. 4-a), which was consistent with the findings at the global scale. The statistical significant critical thresholds of land cover types ranged from 4 to 12°C. In addition to grassland, the sensitivity of the IVTCU to T for the other land cover types was also consistent with that for the global-scale analysis, which included three stages from low to high and again to low sensitivity.

Fig. 4

The trends in the impact of T on the IVTCU in different climate zones significantly varied (Fig. 4-b). The impacts of T on the IVTCU generally decreased with increasing T in two cold zones (e.g., cold dry winter and cold without dry season). The statistical significant critical thresholds were both 8°C. When T was below the threshold, the sensitivity was relatively low, but the influence on the IVTCU was relatively strong, with a mean RRC above 0.68. When T was higher than the threshold, the impact rapidly decreased. In three temperate zones (e.g., temperate dry summer, temperate dry winter, and temperate without dry season), the impact of T on the IVTCU first increased but then decreased with increasing T, with the corresponding statistical significant thresholds being 9, 7, and 5°C, respectively. In the other three climate zones (e.g., arid desert, arid steppe, and tropical savannah), the statistical significant critical thresholds were 6, 12, and 22°C, respectively.

The impact of the VPD on the IVTCU first increased but then decreased with increasing VPD in forests, savannas, and croplands, with the statistical significant critical thresholds being 2.5 or 3.0 hPa (Fig. 4-c). This finding is consistent with that at the global scale. The sensitivity of the IVTCU to the VPD below the threshold was greater than that above the threshold. In grasslands and urban and built-up regions, the impact of the VPD on the IVTCU first remained stable but then decreased, with thresholds of 7.0 and 10.0 hPa, respectively. When the VPD was below the threshold, the sensitivity was relatively low, and the VPD strongly inhibited the IVTCU. When the VPD exceeded the threshold, the inhibitory effect gradually decreased. The trends in the impact of the VPD on the IVTCU were complex in different climate zones (Fig. 4-d). Arid steppe, cold

without dry season and temperate dry summer regions showed consistent trends at the global scale—the impact of the VPD on the IVTCU first increased but then gradually decreased—with statistical significant thresholds of 2.0 hPa and 3.0 hPa, respectively, which were close to the global-scale threshold (2.5 hPa).

DISCUSSION

Early debates on the dominant controlling factors of the IVTCU focused mainly on T or water availability (P and SM). Later, the disputes focused on the VPD and SM. The differences in the data might be the cause of these different results. There is a discrepancy in the VPD calculated from modelled or reanalysed meteorological data products in previous studies and derived from ground observations adopted in this study. The average Kling–Gupta efficiency (KGE) between the best-performing VPD products and the observed values was approximately 0.70, and the KGE of the large-deviation products could be lower than 0.50 (Supplementary Fig. 2-a). Large deviations (KGE<0.60) were located mainly in northern South America, the Mediterranean Sea and the Qinghai–Tibetan Plateau (Supplementary Fig. 2-d to -j). The trend consistency between the best-performing VPD products and the observed values was approximately 80%, and for the poorly performing products, the trend consistency was less than 70% (Supplementary Fig. 3-a). The inconsistencies were observed mainly in North America, northern South America, South Asia, Southeast Asia and the Qinghai–Tibetan Plateau (Supplementary Fig. 3-c to -i). In addition, the application of popular meteorological products, such as MERRA2 and NCEP, in VPD studies requires more caution because of their poor performance, with average KGEs of 0.56 and 0.40, respectively (Supplementary Fig. 2 and Fig. 3).

Significant discrepancies in VPD simulations were also found across different computational methods (Supplementary Figs. 2 and 3). When only minimum (T_n) and maximum (T_x) temperature data were available, the VPD is often obtained by deriving the mean water vapour pressure from T_n and T_x, denoted as $e^o(T_n)$ and $e^o(T_x)$ (equation (4)), respectively, as in previous studies[2,17,24,25]. The accuracy of this method is unsatisfactory, with a median KGE of only 0.77 across all the stations. Stations with poor performance were located mainly in North America and northern South America (Supplementary Fig. 2-d). We found that using the mean of T_n and T_x to approximately estimate the average temperature (T_a) (Equation (3)) significantly improved the VPD accuracy, with the mean KGE increasing to 0.92 (Supplementary Fig. 2-a and -c). The performance of equation (7), in which the VPD is calculated from absolute humidity and atmospheric pressure, is relatively lower than that of the other methods (equations (5) and (6)). This may also explain the low performance of the MERRA2 and NCEP products. The VPDs calculated from the monthly and daily ground observation series showed almost no differences, with both the median and mean KGEs reaching 0.98, which is consistent with the results evaluated by the ERA data[2]. Overall, different data sources and different computational methods would result in different VPD simulations. These differences in VPD simulations might be one of the reasons for the debates on the dominant controlling factors of the IVTCU.

The data we used for evaluating the IVTCU differ from those used in previous research in two key aspects: 1) ground-observed meteorological data, close to true values, were adopted to replace model- or reanalysis-based meteorological products; and 2) remotely sensed GPP data, encompassing diverse trends, were employed to avoid the exclusive use of GPP products with

either increasing or decreasing-trends, as seen in prior studies. On the basis of these findings, this study systematically evaluated the effects of T, the VPD, P and SM on the IVTCU and reemphasized the dominant control of T on the global IVTCU. In general, T and the VPD largely controlled the IVTCU in the Northern Hemisphere and the Southern Hemisphere, respectively. Evaluations based on individual GPP products also confirmed this conclusion. (Supplementary Fig. 5).

Although T is the dominant factor for the global IVTCU, its influence is weaker than that of the VPD in tropical and southern extratropical regions. These findings are similar to those of Wang et al. (2022)[22], who reported greater control of TWS than T in these regions. The reduced influence of T might be associated with the declining dew point temperature and minimum temperature trends in these regions (Supplementary Fig. 4).

It is widely accepted that the IVTCU are either predominantly controlled by water availability (P or SM) in arid land ecosystems[11,12,26] or by T in tropical ecosystems[10,13]. Although the impacts of P and SM on the IVTCU in arid regions were indeed greater than that in other regions, they were weaker than that of the VPD (Fig. 2-a). Our findings indicated that the VPD, rather than water availability, is the dominant factor controlling the IVTCU in arid and semiarid regions, suggesting that the VPD has a stronger inhibitory effect on the IVTCU in drought-adapted ecosystems. Because the influence of the VPD on vegetation is achieved mainly through the regulation of stomatal closure, the stomata of drought-adapted vegetation are more susceptible to the VPD. In addition, compared with other vegetation types, these ecosystems also exhibit relatively small heights. These findings indicate that the VPD more notably influences drought-adapted ecosystems

through the regulation of stomatal closure. Although the VPD dominated the IVTCU in tropical savannas, the results from humid regions indicated that T was the dominant factor (Fig. 2-a and 2-c), which is consistent with the findings of previous studies on humid ecosystems[10,13]. These findings suggested that the IVTCU in humid regions were more sensitive to T than to the VPD. This may be attributed to the fact that vegetation in humid regions is less constrained by water availability, thereby reducing the impact of the VPD on vegetation growth through stomatal regulation. In terms of ecosystem types, the IVTCU in grasslands were predominantly controlled by the VPD, which is consistent with the heightened sensitivity of grasslands to the VPD, especially the strong inhibitory effect of the afternoon VPD on vegetation growth through stomatal closure[27]. The proportion of T-dominant stations was greatest in the forest ecosystem, which was characterized by greater vegetation height than in the other vegetation types, indicating that compared with T, the VPD, which regulates stomatal closure, has a weaker effect on taller vegetation.

Spatially, the dominance of the VPD for the IVTCU was observed across 40–55°N in Eurasia (largely overlapping with arid and semiarid regions), the central and northern United States, South America, and Oceania. This spatial pattern strongly coincides with the VPD-dominant regions identified by Li et al. (2023)[19], who mapped the spatial covariance of T, the VPD, and CO_2 with GPP across global vegetated land. The spatial distribution of the T-dominant region, primarily in the boreal and eastern Chinese regions, was also consistent with that reported by Li et al. (2023)[19]. Given our focus on meteorological factors, the spatial patterns of VPD- and T-dominant regions corresponded with the CO_2 dominance patterns reported by Li et al. (2023)[19], in which T

dominated north of 60°N and the VPD dominated in Northern Hemisphere tropical regions, such as Central Africa, South Asia, and the Indochinese Peninsula.

Neutral or even positive effects of the VPD on vegetation were found in regions with generally low VPD values, such as northern Eurasia[21]. Our partial correlation analysis yielded a similar result: the VPD was positively correlated with GPP in cold regions (Supplementary Fig. 8-b). Rather than attributing this positive relationship solely to low VPD levels, it is more consistent with the low-temperature characteristics of cold regions, suggesting that the VPD plays a facilitating role in shaping the gross carbon uptake in these ecosystems. In addition, the vegetation productivity responded negatively to VPD changes in arid and semiarid zones but responded neutrally or positively in humid zones[21]. However, our findings indicated that positive VPD–GPP correlations were restricted to high-latitude cold regions, with the VPD generally exerting an inhibitory effect on the gross carbon uptake elsewhere (Fig. 1 and Supplementary Fig. 8-b).

The application of partial correlation analysis to identify the dominant controlling factors across land cover types revealed that T and P dominated in boreal and desert regions[4], respectively, which was consistent with our results. However, they reported that P was the dominant factor in grasslands, tropical savannas, and shrublands, whereas our results indicated that the VPD was the dominant factor in these corresponding ecosystems.

Previous studies on the sensitivity and thresholds of the IVTCU to T and the VPD are limited to tropical regions[15,17] and high-latitude regions[21], respectively. We systematically investigated the sensitivity and critical threshold of the IVTCU to T and the VPD at the global scale and across different land cover types and climate zones. This serves as both a validation and a complement to

existing research.

In forests and savannas, the critical threshold of the sensitivity of the IVTCU to T coincides with the mean observed T values within these regions. This indicates that T has an overall strong influence on the IVTCU when it remains below the regional average temperature. However, when T exceeds the average climate level, the sensitivity of the IVTCU to T increases, and the impact of T on the IVTCU decreases sharply with increasing temperature. These findings are consistent with the results for tropical forests[15]. At the global scale, when T exceeds the observed mean temperature (approximately 10°C), the dominant control of the IVTCU shifts from T to the VPD, as the mean RRC of T begins to fall below that of the VPD (approximately 0.40).

This study revealed that T is highly sensitive to the gross carbon uptake of tropical savannahs (Fig. 4b), with its influence decreasing sharply with increasing temperature. The RRC decreases from 0.35 at 20°C to less than 0.10 at 27°C. When T exceeds 28°C, the positive effect of T on the gross carbon uptake of tropical savannahs almost disappears. This finding is similar to the result of tropical biomass productivity revealed by a segmented regression analysis[17], in which a temperature threshold of 29.04°C (±0.05°C) was identified.

Notably, for high-latitude ecosystems, a pronounced shift in the response of vegetation productivity to the VPD occurs during the growing season when the VPD surpasses a threshold of 3.5 to 4.0 hectopascals[21]. This study verifies this, as the thresholds for the two cold regions are identified as 3.0 hPa and 5.0 hPa. In addition, similar thresholds are also found in most other climate zones. These sensitivity and critical threshold analyses might have reference value for carbon sink management.

This study has several limitations. Owing to the relatively high spatial resolution of the grid at 0.05°×0.05°, the observed annual values of ground meteorological variables within the corresponding grid, such as T_a, T_d, and relative humidity (RH), might be sufficient to represent the true values within the grid. However, it should be noted that the observed station values do not fully represent the grid values. This study used meteorological data from 986 ground stations that are distributed globally, which have a certain representativeness of the globe. However, the number of these stations is limited and cannot fully represent the entire globe. If more observations are available, future research could increase the number of observation stations in order to improve their representativeness at the global scale. The gridded meteorological data products with global coverage that are closer to the true values remain an important data source for future related research. The results of this study were compared with those of previous related research. However, the analysis of the potential physical mechanisms that might explain that the consistent or different results were not sufficiently in-depth. More data support and more interpretation would be more meaningful in future research. Because of the lack of global in-situ SM observations, SM data products with relatively high resolution and global coverage are relatively scarce. To maximize the utilization of the collected data, the three types of SM data used are all considered to represent the root layer in this study. If there are more SM data from different depths, considering the impact of SM from different depths on the IVTCU would be interesting for further research. Besides the factors analysed in this study, there are many other factors influencing the IVTCU, such as solar radiation, cloudiness, aerosol effects, CO_2 fertilization, and vegetation cover. If ground observations of these variables are available, the combined influence of more factors on the

IVTCU would be more meaningful in future research. When evaluating the VPD simulations using different reanalysis meteorological data products, the impact of the differences in spatial resolution among these products was not considered in this study. Due to data limitations, this study investigated the controlling factors on the IVTCU by the GPP data from 1982 to 2016. Several studies have shown that the frequency of extreme weather events has increased in recent years[28-30]. These extreme climate changes might have an impact on the IVTCU. If more updated data is available, assessing the impacts of climate change on the IVTCU would be one of the important research directions in the future.

METHODS

Ground-observed meteorological data. We obtained meteorological data from 2,545 ground observation stations, which provided continuous daily records from 1973 to 2024. The dataset included T_a, T_x, T_n, T_d, and P. These data were obtained from the National Oceanic and Atmospheric Administration (NOAA) National Climatic Data Center (NCDC; ftp://ftp.ncdc.noaa.gov/pub/data/gsod). To ensure data quality, outliers were identified and removed using the mean ± 3 standard deviations criterion. The outliers and missing values were subsequently interpolated using linear interpolation. Due to missing values in several GPP data products when covering meteorological stations and strict overlap requirements, 986 sites that had complete intersections with all GPP data products were used for the ridge regression analysis.

Reanalysis meteorological data products. The VPD data derived from ground-based observations were used as a reference to evaluate the performance of six widely used reanalysis

data products for simulating the VPD, namely, CRU, ERA, HadISDH, TerraClimate, MERRA2, and NCEP[31-37]. Detailed information on each product is provided in Supplementary Table 1. For comparison, the grid values corresponding to the locations of the observation stations were extracted and evaluated against the observed values.

Gross carbon uptake GPP data. A total of 18 remote sensing-based and 11 Earth system model-simulated GPP data products (Supplementary Table 2)[38-50] were collected. The TRENDY-v12 GPP products under scenario S3 containing all forcings, i.e., CO_2 concentration, climate and land use change, were used in this study. Nine GPP products (Supplementary Table 2) with long temporal coverage and an integration of both remote sensing and eddy covariance (EC) observations were used for the impact assessment of the IVTCU. These included three products based on light use efficiency (LUE) models combined with EC observations and remote sensing data[38, 39, 42], three products derived from machine learning models integrated with EC and remote sensing data[43], and one product based on solar-induced chlorophyll fluorescence[46]. These products have demonstrated strong abilities to capture interannual variations in GPP at both site and global scales[38, 39, 42, 43, 46]. The FluxCom_CRUJRA, FluxCom_ERA5, and LUE products were resampled (bilinear interpolation) to a 0.05° spatial resolution to match the other datasets. The data series after resampling have high degrees of consistency with the original values. The mean KGE values for all stations corresponding to the three products are 0.94, 0.94, and 0.93 respectively (Supplementary Fig. 9). All the data series were standardized to minimize inconsistencies and biases across the GPP products. Finally, an ensemble mean was calculated from the standardized anomalies of the nine products for the period 1982–2016 and used in the impact assessment of the

IVTCU. The growing season (temperature > 0 °C) GPP data were used in this study.

SM data. Three SM data products (Supplementary Table 3) were applied to assess the impact of moisture on the IVTCU. ERA and TerraClimate are reanalysis datasets[32, 35], whereas GLEAM is a remote sensing-based product[51]. All SM products were resampled (bilinear interpolation) to a 0.05° spatial resolution to match the GPP datasets.

Ridge regression analysis. To address the multicollinearity among the independent variables, we applied ridge regression to assess the effects of T, the VPD, P, and SM on the interannual variations in GPP. Ridge regression is a linear regression technique that introduces a regularization term into the regression model to reduce the size of regression coefficients, thereby mitigating the effects of multicollinearity[52]. This method effectively addresses the problem of parameter estimation bias caused by high correlation among independent variables by introducing a regularity term. Constraining the magnitude of regression coefficients reduces model variance and enhances the stability and reliability of multidimensional models. It has been widely and successfully applied in studies on the impact of independent variables with multicollinearity on ecosystems[21,53-55]. The regularization parameter (λ) was automatically determined through 5-fold cross-validation, which achieves this by minimizing the prediction error. This is a standard procedure that ensures the selection of a robust λ value that enhances the generalizability of the model[56]. This cross-validation process also serves as a key assessment of coefficient stability and model performance[57]. Grid-based GPP and SM data series corresponding to the locations of the meteorological stations and the station-based T, VPD, and P data series were used as inputs for the ridge regression models. Before the ridge regression was conducted, annual data series of all the input variables were

standardized by dividing the anomalies by their standard deviations for the period from 1982 to 2016, which is also referenced as the z-scores method[58]. In addition, the standardized data series were also detrended for the ridge regression.

Partial correlation analysis: Partial correlation analysis can be used to analyse the correlation between two variables while controlling for the influence of other variables and therefore to avoid interference from other variables. To evaluate the relationship between the VPD and GPP, partial correlation analyses were used to exclude the effects of T and P. This statistical method is widely applied to isolate the relationship between two variables from the confounding effects of other correlated variables [4,53,59].

Multiple VPD calculation methods. The VPD is defined as the difference between the saturated vapour pressure (SVP) and actual vapour pressure (AVP). The SVP is calculated using either T_a or the combination of T_x and T_n. The AVP can be derived from T_d, RH, or specific humidity (SH) and atmospheric pressure (AP). Therefore, there are six potential combinations for calculating the VPD: T_a combined with T_d, RH, or specific humidity and pressure and $(T_x–T_n)/2$ replacing Ta and combined with T_d, RH, or SH and AP.

The VPD is calculated as follows:

$$\mathrm{VPD} = \mathrm{SVP} - \mathrm{AVP} \quad (1)$$

$$\mathrm{SVP} = \begin{cases} e^o(T_a) = 0.6108 \times \exp\left(\dfrac{17.27 \times T_a}{T_a + 237.3}\right) & (2) \\ e^o(0.5 \times (T_n + T_x)) = 0.6108 \times \exp\left(\dfrac{17.27 \times 0.5 \times (T_n + T_x)}{0.5 \times (T_n + T_x) + 237.3}\right) & (3) \\ 0.5 \times [e^o(T_n) + e^o(T_x)] = 0.5 \times \left[\begin{array}{l} 0.6108 \times \exp\left(\dfrac{17.27 \times T_n}{T_n + 237.3}\right) \\ +0.6108 \times \exp\left(\dfrac{17.27 \times T_x}{T_x + 237.3}\right) \end{array}\right] & (4) \end{cases}$$

$$\mathrm{AVP} = \begin{cases} e^o(T_d) = 0.6108 \times \exp\left(\dfrac{17.27 \times T_d}{T_d + 237.3}\right) & (5) \\ \dfrac{RH}{100} \times SVP & (6) \\ \dfrac{SH \times AP}{(0.622 + SH \times 0.378) \times 1000} & (7) \end{cases}$$

where AVP (kPa), SVP (kPa), T_a (°C), T_n (°C), T_x (°C), T_d (°C), RH (%), SH (kg kg^{-1}), and AP (Pa) are the actual vapour pressure, saturated vapour pressure, average, minimum, and maximum temperatures, dew point temperature, mean relative humidity, specific humidity, and atmospheric pressure, respectively.

Evaluation of the VPD simulations. We used the VPD values calculated from the daily T_a and T_d data series from ground observations as a reference to evaluate the performance of the six commonly used reanalysis data products in simulating the VPD. The variables used by each product for the VPD calculation are described in Supplementary Table 1. In addition, we assessed the discrepancies among different VPD calculation methods. Given that some commonly used meteorological data products provide only monthly data, we also compared the differences in the VPD estimates derived from daily versus monthly data. KGE[60], which integrates the correlation coefficient, relative error and standard deviation, was used as the evaluation criterion.

Trend and critical thresholds detection methods. The rank-based nonparametric Mann–Kendall test and trend magnitude method[61] were applied to detect long-term monotonic trends and their

magnitudes. This test can resolve nonnormality, censoring, data reported as less-than values, missing values and seasonality; it also has high asymptotic efficiency[62]. The Piecewise Regression method was applied to detect critical threshold inflection points in the sensitivity of the IVTCU to T and the VPD. The significance level (α) was defined as $\alpha = 0.05$.

Data availability

A map of climate zones is available at http://www.hydrol-earth-syst-sci.net/11/1633/2007/hess-11-1633-2007-supplement.zip (ref. [63]). Land cover maps are available at https://www.earthdata.nasa.gov/ (ref. [64]). All other datasets used in this study are publicly available from the referenced sources: reanalysis meteorological products[31-37], GPP products[38-50], and SM products[32,35,51].

References

1. Green, J. K. et al. Large influence of soil moisture variability on long-term terrestrial carbon uptake. Nature **565**, 476–479 (2019).

2. He, B. et al. Worldwide impacts of atmospheric vapor pressure deficit on the interannual variability of terrestrial carbon sinks. Natl. Sci. Rev. **9**, nwab150 (2022).

3. Humphrey, V. et al. Soil moisture-atmosphere feedback dominates land carbon uptake variability. Nature **592**, 65–69 (2021).

4. Beer, C. et al. Terrestrial gross carbon dioxide uptake: global distribution and covariation with climate. Science **329**, 834–838 (2010).

5. Liu, Z. et al. Precipitation thresholds regulate net carbon exchange at the continental scale. Nat. Commun. **9**, 3596 (2018).

6. Zhang, W. et al. Recent decrease of the impact of tropical temperature on the carbon cycle linked to increased precipitation. Nat. Commun. **14**, 965 (2023).

7. Chen, Z., Wang, W., Forzieri, G. & Cescatti, A. Transition from positive to negative indirect CO_2 effects on the vegetation carbon uptake. Nat. Commun. **15**, 1500 (2024).

8. Wang, X. H. et al. A two-fold increase of carbon cycle sensitivity to tropical temperature variations. Nature **506**, 212–215 (2014).

9. Jung, M. et al. Compensatory water effects link yearly global land CO_2 sink changes to temperature. Nature **541**, 516–520 (2017).

10. Ahlström, A. et al. The dominant role of semi-arid ecosystems in the trend and variability of the land CO_2 sink. Science **348**, 895–899 (2015).

11. Poulter, B. et al. Contribution of semi-arid ecosystems to interannual variability of the global carbon cycle. Nature, **509**, 600–603 (2014).

12. Liu, L. et al. 2020. Soil moisture dominates dryness stress on ecosystem production globally. Nat. Commun. **11**, 4892 (2020).

13. Anderegg, W. R. L. et al. Tropical nighttime warming as a dominant driver of variability in the terrestrial carbon sink. Proc. Natl Acad. Sci. USA **112**, 15591–15596 (2015).

14. Yuan, W. et al. Increased atmospheric vapor pressure deficit reduces global vegetation growth. Sci. Adv. **5**, eaax1396 (2019).

15. Smith, M. N. et al. Empirical evidence for resilience of tropical forest photosynthesis in a warmer world. Nat. Plants **6**, 1225–1230 (2020).

16. Fu, Z. et al. Atmospheric dryness reduces photosynthesis along a large range of soil water deficits. Nat. Commun. **13**, 989 (2022).

17. Nölte A., Yousefpour R., Cifuentes-Jara M. & Hanewinkel M. Sharp decline in future productivity of tropical reforestation above 29°C mean annual temperature. Sci. Adv. **9**, eadg917 (2023).

18. Konings, A. G., Williams, A. P. & Gentine, P. Sensitivity of grassland productivity to aridity controlled by stomatal and xylem regulation. Nat. Geosci. **10**, 284–288 (2017).

19. Li, F. et al. Global water use efficiency saturation due to increased vapor pressure deficit. Science **381**, 672–677 (2023).

20. Chen, N. et al. Warming-induced vapor pressure deficit suppression of vegetation growth diminished in northern peatlands. Nat. Commun.**14**, 7885 (2023).

21. Zhong, Z. et al. Disentangling the effects of vapor pressure deficit on northern terrestrial vegetation productivity. Sci. Adv. **9**, eadf3166 (2023).

22. Wang, K. et al. Regional and seasonal partitioning of water and temperature controls on global land carbon uptake variability. Nat. Commun. **13**, 3469 (2022).

23. Lu, H. et al. Large influence of atmospheric vapor pressure deficit on ecosystem production efficiency. Nat. Commun. **13**, 1653 (2022).

24. Allen, R. G., Pereira, L. S., Raes, D. & Smith, M. Crop evapotranspiration: Guidelines for computing crop water requirements. FAO Irrigation and Drainage Paper 56, Rome, Italy, pp. 18–37 (1998).

25. Kath, J. et al. Vapour pressure deficit determines critical thresholds for global coffee production under climate change. Nat. Food **3**, 871–880 (2022).

26. Seddon, A. W. R., Macias-Fauria, M., Long, P. R., Benz, D. & Willis, K. J. Sensitivity of global terrestrial ecosystems to climate variability. Nature, **531**, 229–232 (2016).

27. Niu, S.L. et al. Temperature responses of ecosystem respiration. Nat. Rev. Earth Environ. **5**, 559–571 (2024).

28. Liu, F., et al. Intraseasonal variability of global land monsoon precipitation and its recent trend. npj Clim. Atmos. Sci. **5**, 30 (2022).

29. Feldman, A., et al. Large global-scale vegetation sensitivity to daily rainfall variability. Nature **636**, 380–384 (2024).

30. Li, J., Wang, S., Zhu, J., Wang, D., Zhao, T. Accelerated shifts from heatwaves to heavy rainfall in a changing climate. npj Clim. Atmos. Sci. **8**, 214 (2025).31. Harris, I., Osborn, T. J., Jones, P. & Lister, D. Version 4 of the CRU TS monthly high-resolution gridded multivariate climate dataset. Sci. Data **7**, 109 (2020).

32. Muñoz Sabater, J. et al. ERA5-land post-processed daily-statistics from 1950 to present. https://doi.org/10.24381/cds.e9c9c792 (2024).

33. Willett, K. M. et al. HadISDH land surface multi-variable humidity and temperature record for climate monitoring. Clim. Past, **10**, 1983–2006 (2014).

34. Smith, A., Lott, N. & Vose, R. The integrated surface database: recent developments and partnerships. Bull. Am. Meteorol. Soc. **92**, 704–708 (2011).

35. Abatzoglou, J., Dobrowski, S., Parks, S. & Hegewisch, K. C. TerraClimate, a high-resolution

global dataset of monthly climate and climatic water balance from 1958–2015. Sci. Data **5**, 170191 (2018).

36. Gelaro, R. et al. The Modern-Era Retrospective Analysis for Research and Applications, Version 2 (MERRA-2). J. Climate **30**, 5419–5454 (2017).

37. Kanamitsu, M., Ebisuzaki, W., Woollen, J., Yang, S. K. & Potter, G. L. NCEP–DOE AMIP-II reanalysis (R-2). Bull. Am. Meteorol. Soc. **83**, 1631–1644 (2002).

38. Yuan, W.P. et al. Deriving a light use efficiency model from eddy covariance flux data for predicting dailygross primary production across biomes. Agric. For. Meteorol. **143**, 189–207 (2007).

39. Zheng, Y. et al. Improved estimate of global gross primary production for reproducing its long-term variation, 1982-2017. figshare https://doi.org/10.6084/m9.figshare.8942336.v3 (2019).

40. Jung, M. et al. The FLUXCOM ensemble of global land-atmosphere energy fluxes. Sci. Data **6**, 74 (2019).

41. Li, X. & Xiao, J. Mapping photosynthesis solely from solar-induced chlorophyll fluorescence: A global, fine-resolution dataset of gross primary production derived from OCO-2. Remote Sens. **11**, 2563 (2019).

42. Madani, N. & Parazoo, N. C. Global Monthly GPP from an Improved Light Use Efficiency Model, 1982-2016. ORNL DAAC, Oak Ridge, Tennessee, USA https://doi.org/10.3334/ORNLDAAC/1789 (2020).

43. Li, F. et al. Global water use efficiency saturation due to increased vapor pressure deficit. Science **381**, 672–677 (2023).

44. Zhao, M., Heinsch, F. A., Nemani, R. R. & Running., S. W. Improvements of the MODIS terrestrial gross and net primary production global data set. Sci. Total Environ. **95**, 164–176 (2005).

45. Yuan, Q. & Wang, X. Global carbon cycle dataset (2000-2023). National Tibetan Plateau/Third Pole Environment Data Center https://doi.org/10.11888/Terre.tpdc.301530 (2024).

46. Wang, S., Zhang, Y., Ju, W., Qiu, B. & Zhang, Z. Tracking the seasonal and inter-annual variations of global gross primary production during last four decades using satellite near-infrared reflectance data. Sci. Total Environ. **755**, 142569 (2021).

47. Stocker, B. D. et al. Drought impacts on terrestrial primary production underestimated by satellite monitoring. Nat. Geosci. **12**, 264–270 (2019).

48. Zhang, Y. et al. Multi-decadal trends in global terrestrial evapotranspiration and its components. Sci. Rep. **6**, 19124 (2016).

49. Friedlingstein, P. et al. Global carbon budget 2024. Earth Syst. Sci. Data **17**, 965–1039 (2025).

50. Zhang, Y. et al. A global moderate resolution dataset of gross primary production of vegetation for 2000–2016, Sci. Data **4**, 170165 (2015).

51. Hulsman, P., Keune, J., Koppa, A., Schellekens, J. & Miralles, D. G. Incorporating plant access to groundwater in existing global, satellite-based evaporation estimates. Water Resour. Res. **59**, e2022WR033731 (2023).

52. Hoerl, A. E. & Kennard, R. W. Ridge regression-biased estimation for nonorthogonal problems. Technometrics **12**, 55–67 (1970).

53. Peng, S. et al. Asymmetric effects of daytime and night-time warming on Northern Hemisphere

vegetation. Nature **501**, 88–92 (2013).

54. Wang, X., Ciais, P., Wang, Y., & Zhu, D. Divergent response of seasonally dry tropical vegetation to climatic variations in dry and wet seasons. Glob. Chang. Biol. **24**, 4709–4717 (2018).

55. Chen, X. et al. Summer atmospheric drying could contributemore to soil moisture change than spring vegetation greening. npj Clim. Atmos. Sci. **7**, 296 (2024).

56. Homaida, A., Pekalp, M. H., & Ebegil, M. Efficient k value computation for enhanced fuzzy ridge regression. J. Comput. Appl. Math. **472**, 116813 (2026).

57. Pohjankukka, J., Pahikkala, T., Nevalainen, P., & Heikkonen, J. Estimating the prediction performance of spatial models via spatial k-fold cross validation. Int. J. Geogr. Inf. Sci. **31**, 2001–2019 (2017).

58. Zhong et al.. Sub-diurnal asymmetric warming has amplified atmospheric dryness since the 1980s. Nat. Commun. **16**, 8247 (2025).

59. Wang, T. et al. Emerging negative impact of warming on summer carbon uptake in northern ecosystems. Nat. Commun. **9**, 5391 (2018).

60. Gupta, H. V., Kling, H., Yilmaz, K. K. & Martinez, G. F. Decomposition of the mean squared error and NSE performance criteria: Implications for improving hydrological modeling. J. Hydrol. **377**, 80–91 (2009).

61. Hirsch, R. M., Slack, J. R., & Smith, R. A. Techniques of trend analysis for monthly water quality data. Water Resour. Res. **18**, 107–121 (1982).

62. Xu, Z. X., Liu, Z. F., Fu, G. B., & Chen, Y. N. Hydro-climate trends of the Tarim River basin

for the last 50 years. J. Arid. Environ. **74**, 256–267 (2010).

63. Peel M. C., Finlayson B. L. & McMahon T. A. 2007. Updated world map of the Köppen-Geiger climate classification. Hydrol. Earth Syst. Sci. **11**, 1633–1644 (2007).

64. Friedl, M. & Sulla-Menashe, D. MODIS/Terra+Aqua Land Cover Type Yearly L3 Global 0.05Deg CMG V061 [Data set]. NASA Land Processes Distributed Active Archive Center https://doi.org/10.5067/MODIS/MCD12C1.061 (2022).

Figure legends

Fig. 1 | Spatial patterns of the dominant factors affecting the IVTCU according to ground meteorological observations. Spatial distribution of the RRCs between the ensemble mean GPP data series and the ground-observed VPD (**a**), P (**b**), and T (**c**) data series. **e**, **f**, and **g** are the corresponding latitudinal distribution patterns. **d** Spatial distribution of the dominant factors (VPD, P, or T) on the IVTCU.

Fig. 2 | Dominant factors of the IVTCU by land cover and climate zone. **a** The RRCs between the ensemble mean GPP series and the VPD, P, and T data series for each climate zone. AD, AS, CDS, CDW, CWDS, Polar, TDS, TDW, TM, TS, and TWDS represent the arid desert, arid steppe, cold dry summer, cold dry winter, cold without dry season, polar, temperate dry summer, temperate dry winter, tropical monsoon, tropical savannah, and temperate without dry season zones, respectively. **b** As in (**a**) but for land cover zones. **c** Proportions of dominant controlling factors in each climate zone. **d** As in (**c**) but for land cover zones.

Fig. 3 | Sensitivity of the IVTCU to T and the VPD and their critical thresholds. a RRCs between the ensemble mean GPP series and T data series at each station under the constraints of

each T bin. **b** As in (**a**) but for the VPD.

Fig. 4 | Sensitivity of the IVTCU to T and the VPD and their critical thresholds in land cover and climate zones. a The mean RRCs of all observed stations between the ensemble mean GPP series and T (**a**) and the VPD (**c**) data series constrained by each calculated bin in land cover types. **b** and **d** are the same as in (**a**) and (**c**) but for climate zones.

ACKNOWLEDGMENT

This study was supported and funded by the National Natural Science Foundation of China (Grant No. 52130907).

AUTHOR CONTRIBUTIONS

Z. Liu; D.J.; and J.W. conceived, designed and wrote the main manuscript. Z. Liu; Z.Y.; M.H.; X.Z.; and X.Y. conducted the analyses. J.L. and Z. Li retrieved and processed the climate and remote sensing data. All authors reviewed the manuscript.

COMPETING INTERESTS

The authors declare no competing financial or non-financial interests.

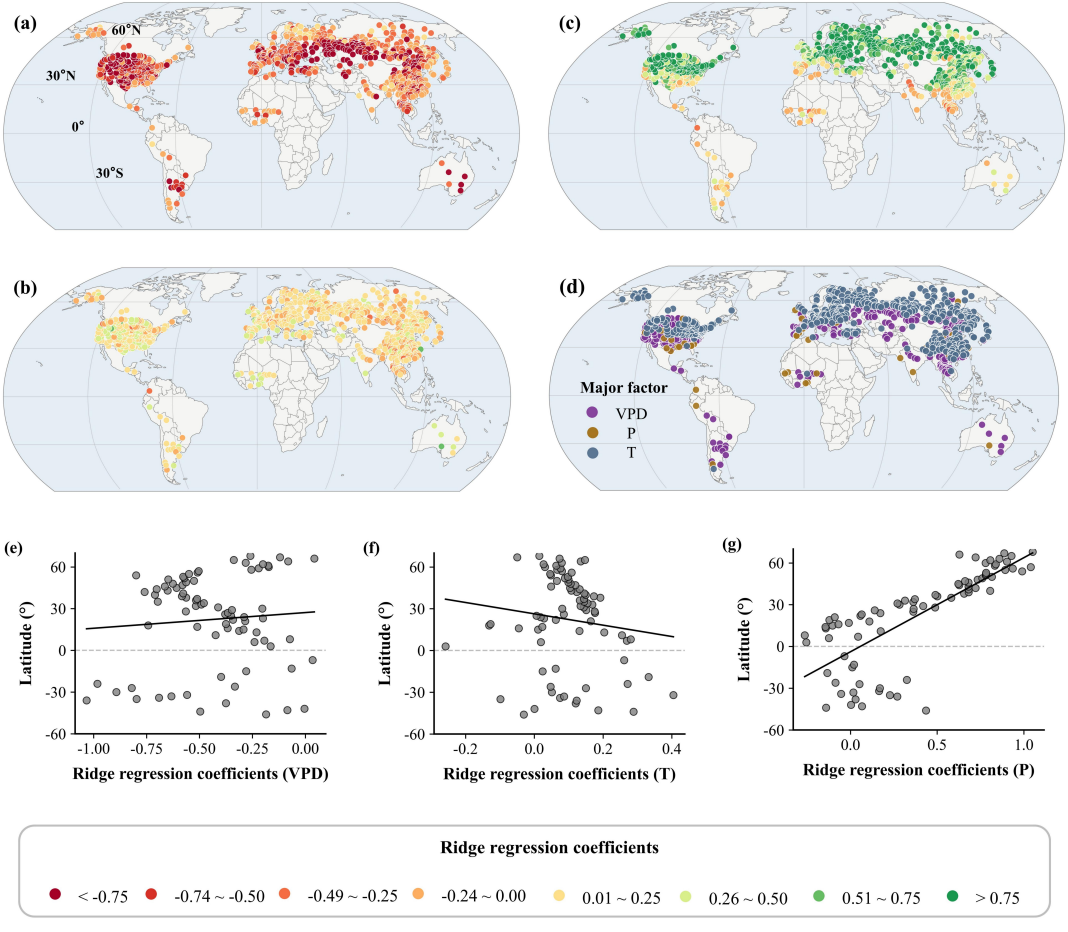
(a)
60°N
30°N
0°
30°S
(b)
(c)
(d)
Major factor
VPD
P
T
(e)
Latitude (°)
Ridge regression coefficients (VPD)
(f)
Latitude (°)
Ridge regression coefficients (T)
(g)
Latitude (°)
Ridge regression coefficients (P)
Ridge regression coefficients
< -0.75
-0.74 ~ -0.50
-0.49 ~ -0.25
-0.24 ~ 0.00
0.01 ~ 0.25
0.26 ~ 0.50
0.51 ~ 0.75
> 0.75

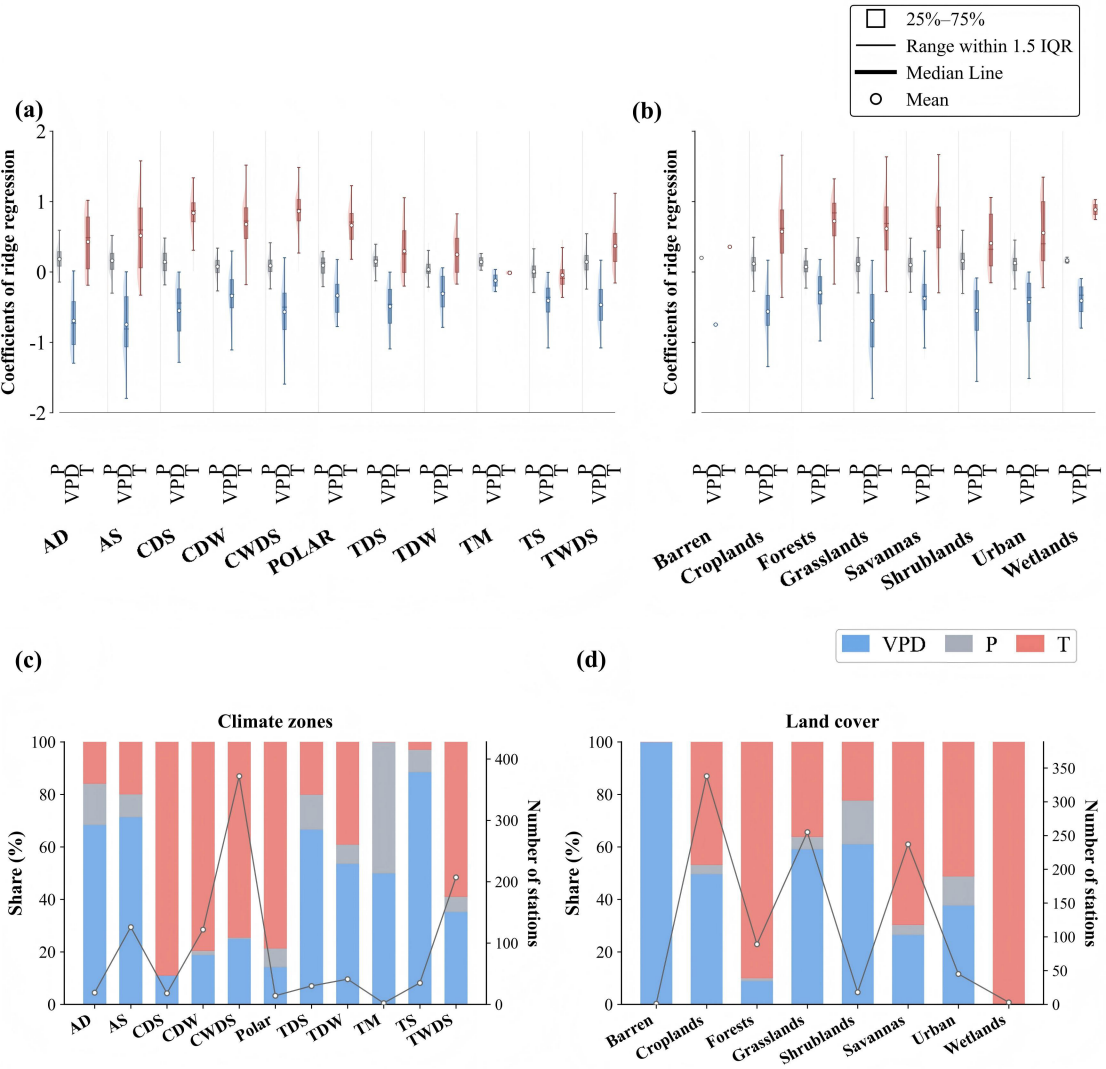

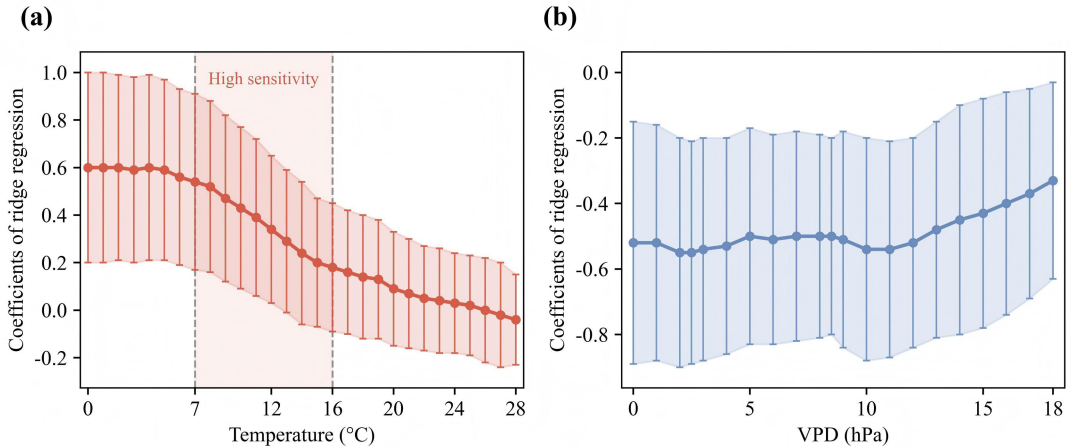

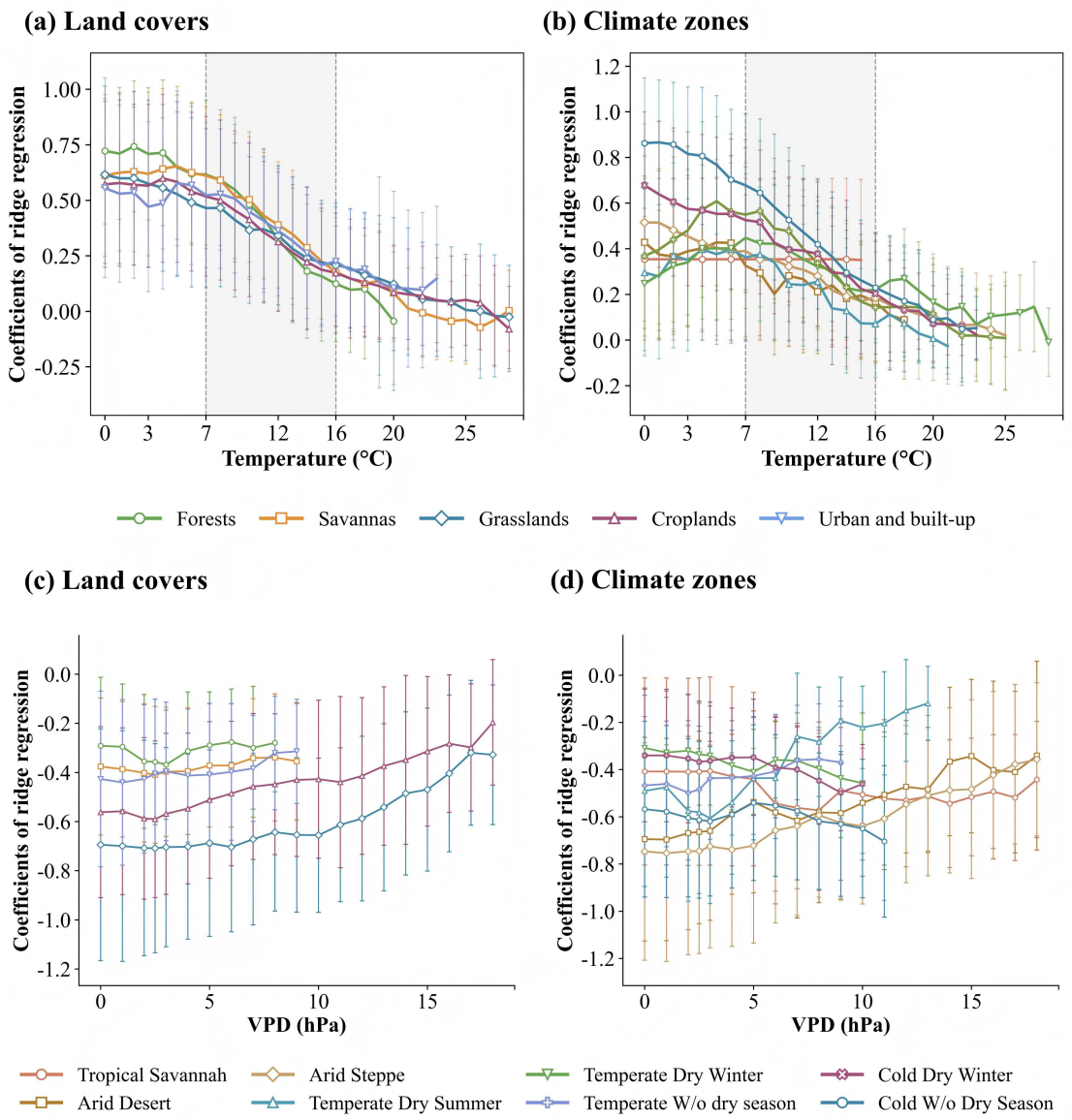
(a) Land covers
(b) Climate zones
Coefficients of ridge regression
Temperature (°C)
Forests
Savannas
Grasslands
Croplands
Urban and built-up
(c) Land covers
(d) Climate zones
VPD (hPa)
Tropical Savannah
Arid Steppe
Temperate Dry Winter
Cold Dry Winter
Arid Desert
Temperate Dry Summer
Temperate W/o dry season
Cold W/o Dry Season